


# Effect of phase contrast and inclusion shape on the effective response of viscoelastic composites using peridynamic computational homogenization theory

Yakubu Kasimu Galadima<sup>a,b</sup>, Selda Oterkus<sup>a</sup> , Erkan Oterkus<sup>a</sup>, Islam Amin<sup>a,c</sup>, Abdel-Hameed El-Aassar<sup>d</sup>, and Hosam Shawky<sup>d</sup>

<sup>a</sup>PeriDynamics Research Centre, Department of Naval Architecture, Ocean and Marine Engineering, University of Strathclyde, Glasgow, UK; <sup>b</sup>Department of Civil Engineering, Ahmadu Bello University, Zaria, Nigeria; <sup>c</sup>Department of Naval Architecture and Marine Engineering, Port Said University, Port Said, Egypt; <sup>d</sup>Egypt Desalination Research Centre of Excellence (EDRC) and Hydrogeochemistry Department, Desert Research Centre, Cairo, Egypt

## ABSTRACT

Viscoelastic composites are widely used in engineering applications, necessitating a comprehensive understanding of their effective response to external loads. This study employs peridynamic computational homogenization theory to investigate the influence of phase contrast and inclusion shape on the effective properties of these composites. By focusing on a two-phase matrix-inclusion composite material and considering circular and elliptical inclusion shapes, this study explores the relationship between these factors and the resulting effective behavior. The simulation results demonstrate that the use of circular inclusions result in isotropic effective response of the composites for all values of phase contrasts, while elliptical inclusions lead to an increase in anisotropy as phase contrast increases. These findings highlight the significant impact of inclusion shape and phase contrast on the effective behavior of composites.

## ARTICLE HISTORY

Received 11 April 2023  
Accepted 22 May 2023

## KEYWORDS

Peridynamics; non-ordinary state-based correspondence model; viscoelasticity; anisotropy; composite; effective behavior

## 1. Introduction



Understanding how materials respond to external loads is essential in the design of engineering systems. As composite systems made of viscoelastic materials, such as polymers, are increasingly gaining prominence across a wide spectrum of applications in the civil, aerospace, and medical device industries, it is necessary to understand the effective response of the composite system. One crucial aspect that can affect the effective response is the inclusion shape, which can vary widely during the production process [1]. To meet specific property requirements, it is therefore necessary to investigate the nature and degree of the influence of inclusion shape on the effective response of the composite system. Additionally, the difference in physical properties between the matrix and the inclusion, known as phase contrast, is also a critical factor that can affect the effective response of the composite system.

Phase contrast has been established as a key factor that influences the regulation of elastic properties in composites, as evidenced by previous studies. As one such study [2] has shown, Poisson's effect plays a critical role in the regulation of the elastic properties of composites, with phase contrast identified as a driving mechanism. In particular, the study found that during deformation of a composite system, Poisson's effect induces

secondary strains and stresses into the phase material, requiring more strain energy to achieve the same deformation in the primary direction and increasing the stiffness of the composite system. Moreover, the increased stiffness was found to depend on the contrast of phase properties.

Based on these findings, the current research aims to investigate the influence of inclusion shape and phase contrast on the effective response of viscoelastic composites within the Peridynamic modeling framework. This represents a significant contribution to an ongoing research effort aimed at verifying, demonstrating, and extending the capabilities of a nonlocal first order Peridynamic Computational Homogenization Theory (PDCHT) [3] previously proposed by the authors. As a computational tool that allows the bridging of gap between microstructural characteristics and macroscopic response the PDCHT has been shown to be a powerful tool for understanding the intricate interactions within heterogenous materials especially in the presence of discontinuous response [4] and nonlocal viscoelastic response [5].

Computational methods based on classical continuum mechanics (CCM) have for long been the standard methods for the characterization of elastic composites [6,7] and viscoelastic composites [8–10]. However, CCM has difficulties in modeling discontinuous behavior, such as dynamic cracks, because its

**CONTACT** Selda Oterkus  [selda.oterkus@strath.ac.uk](mailto:selda.oterkus@strath.ac.uk)  PeriDynamics Research Centre, Department of Naval Architecture, Ocean and Marine Engineering, University of Strathclyde, Glasgow, UK.

© 2023 The Author(s). Published with license by Taylor & Francis Group, LLC

This is an Open Access article distributed under the terms of the Creative Commons Attribution-NonCommercial License (<http://creativecommons.org/licenses/by-nc/4.0/>), which permits unrestricted non-commercial use, distribution, and reproduction in any medium, provided the original work is properly cited. The terms on which this article has been published allow the posting of the Accepted Manuscript in a repository by the author(s) or with their consent.

mathematical framework is based on differential equations that describe the rate of change of the displacement or deformation gradient field at each point in space. This is because the derivative of the displacement field at discontinuities is ill-defined. Another significant limitation of CCM is its inability to capture nonlocal behavior, such as size effect and material softening due to damage. CCM assumes local action, which presupposes that the behavior of a material at a point is only influenced by the state of the material at that point.

Given these limitations of CCM in modeling discontinuous behavior, Peridynamic theory (PD) was proposed [11] as a nonlocal alternative. To address the outlined limitations of the CCM, the PD theory uses integral operators instead of differential operators. This approach allows PD to model the evolution of discontinuous behavior in a more natural and intuitive way. In PD, the deformation at each point is related to the deformation in a finite neighborhood of that point, rather than the deformation gradient field at that point alone. This allows PD to capture the propagation of cracks and other discontinuities using the same fundamental equation of motion. Furthermore, integral operators endow the theory with the additional capability to account for phenomena driven by nonlocal behavior, such as size effect and material softening due to damage. In PD, the deformation at each point is influenced not only by the stress and strain at that point but also by the stress and strain in a neighborhood around that point. This neighborhood is termed as the horizon, and its size can be adjusted to capture the desired length scale of the nonlocal behavior.

Peridynamics has been used to model a wide range of problems in solid mechanics. It has been applied to modeling of fracture processes [12–22], wave propagation and dispersion [23–28], model order reduction [29–32] and homogenization of heterogeneous materials [3–5, 33,34]. Peridynamics has also been applied to characterize viscoelastic [35–37] and plastic [38,39] response of materials.

## 2. Theoretical framework

### 2.1. State-based peridynamic theory

In peridynamics, the state of a primary point situated at position  $\mathbf{x}$  in the reference configuration of a body  $\mathcal{B}$  is determined through the aggregation of interactions between the primary point and a set of secondary points  $\mathbf{x}'$  located within a finite distance  $\delta$ , referred to as the horizon. The relative position  $\xi = \mathbf{x}' - \mathbf{x}$  in the reference configuration is called the *bond length* or simply *bond* while  $\eta = \mathbf{u}'(\mathbf{x}') - \mathbf{u}(\mathbf{x})$  is the relative position in the deformed configuration.

The set  $\mathcal{B}_\delta$  such that

$$\mathcal{B}_\delta(\mathbf{x}) = \{\mathbf{x}' \in \mathcal{R} : |\mathbf{x}' - \mathbf{x}| < \delta\} \quad (1)$$

is called the family of  $\mathbf{x}$  and contain all the points  $\mathbf{x}'$  that interacts with  $\mathbf{x}$ . On the other hand, the set  $\mathcal{H}_\mathbf{x}$  such that

$$\mathcal{H}_\mathbf{x} = \{\xi \in (\mathbb{R} \setminus 0) | (\xi + \mathbf{x}) \in (\mathcal{B}_\delta(\mathbf{x}) \cap \mathcal{B})\} \quad (2)$$

is the family of bonds for point  $\mathbf{x}$ . The equation of motion that tracks the state of a material point  $\mathbf{x}$  in peridynamics is given by the integro-differential equation:

$$\rho \ddot{\mathbf{u}}(\mathbf{x}, t) = \int_{\mathcal{H}_\mathbf{x}} \mathbf{f}(\mathbf{x}', \mathbf{x}, t) d\mathbf{x}' + \mathbf{b}(\mathbf{x}, t) \quad \forall \mathbf{x} \in \mathcal{B}, t \geq 0 \quad (3)$$

where  $\mathbf{u}(\mathbf{x}, t)$  is the displacement vector of point  $\mathbf{x}$  at time  $t$ ,  $\mathbf{f}(\mathbf{x}', \mathbf{x}, t)$  is a vector-valued function that represents the pair-wise force density that  $\mathbf{x}'$  exerts on  $\mathbf{x}$  and  $\mathbf{b}(\mathbf{x}, t)$  is the body force density at point  $\mathbf{x}$ . Through an appropriate material model, the pair-wise force,  $\mathbf{f}$  is expressed as a function of the deformation of all  $\mathbf{x}' \in \mathcal{H}_\mathbf{x}$ . There are two main categories of material models in Peridynamics, viz, the *bond-based* and the *state-based* peridynamic material models. The bond-based model represents the simplest material model in the peridynamic framework, in which each bond connected to a primary point  $\mathbf{x}$  responds independently of all other bonds within the family of  $\mathbf{x}$ . Furthermore, the pairwise force induced in a bond because of deformation is parallel to the bond in the deformed configuration. Due to these postulations, it has been demonstrated that the elastic response of a bond-based material model invariably yields a Poisson's ratio of 1/3 for 2D isotropic solids and 1/4 for 3D isotropic solids. This restriction on the Poisson's ratio in bond-based models limits the range of material behaviors that can be reproduced.

The state-based framework represents efforts for overcoming the limitations of the bond-based framework and presents a framework that can model generalized material response. In the state-based formulation, the response of a bond is contingent upon the deformation of all bonds within a family. This approach eliminates the constraint on the Poisson's ratio and extends the ability of peridynamics to simulate materials with a Poisson's ratio covering the entire permissible range. This is achieved by the introduction of mathematical objects known as states, which are functions defined on  $\mathcal{H}$ . Let  $\mathcal{L}_m$  be a set of all tensors of order  $m$ , then a peridynamic state of order  $m$  associated with a point  $\mathbf{x}$  is a function  $\mathbf{A}(\cdot) : \mathcal{H} \rightarrow \mathcal{L}_m$ , where the angle brackets denote the bond acted upon by the state. A scalar state is a state that maps vectors in  $\mathcal{H}$  to a scalar, while a vector state is a state that maps vectors in  $\mathcal{H}$  to vectors. The set of all peridynamic states of order  $m$  is represented by  $\mathcal{A}_m$ . Hence, if we denote the set of all scalar states by  $\mathcal{S}$ , then  $\mathcal{S} = \mathcal{A}_1$ . Similarly, if the set of all vector states is denoted by  $\mathcal{V}$ , then  $\mathcal{V} = \mathcal{A}_2$ . The most important states in the development of the state-based peridynamics are the deformation state and the force state. A deformation state  $\mathbf{Y}$  maps any bond  $\xi = \mathbf{x}' - \mathbf{x}$  in  $\mathcal{H}$  onto its image under the deformation. The image of  $\xi$  in the deformed configuration when acted upon by  $\mathbf{Y}$  is given by:

$$\mathbf{Y}[\mathbf{x}, t](\mathbf{x}' - \mathbf{x}) = \mathbf{y}'(\mathbf{x}', t) - \mathbf{y}(\mathbf{x}, t) \quad (4)$$

where  $\mathbf{y}'(\mathbf{x}', t)$  and  $\mathbf{y}(\mathbf{x}, t)$  are respectively the position vectors of the points  $\mathbf{x}'$  and  $\mathbf{x}$  in the deformed configuration at time  $t$ . A force state,  $\mathbf{T}$  on the other hand, is a function that associates a force density vector  $\mathbf{t}$  to each bond in  $\mathcal{H}$ , such that:

$$\mathbf{T}[\mathbf{x}, t](\mathbf{x}' - \mathbf{x}) = \mathbf{t}(\mathbf{x}', \mathbf{x}, t) \quad (5)$$

where  $\mathbf{t}(\mathbf{x}', \mathbf{x}, t)$  represents a force interaction between  $\mathbf{x}$  and  $\mathbf{x}'$  due to the force state at  $\mathbf{x}$ . From the requirement for

balance of linear momentum, the pair-wise force density function  $\mathbf{f}$  in (3) is shown [40] to be:

$$\mathbf{f}(\mathbf{x}, \mathbf{x}', t) = \mathbf{T}[\mathbf{x}, t] \langle \mathbf{x}' - \mathbf{x} \rangle - \mathbf{T}[\mathbf{x}', t] \langle \mathbf{x} - \mathbf{x}' \rangle \quad (6)$$

where  $\mathbf{T}[\mathbf{x}, t]$  and  $\mathbf{T}[\mathbf{x}', t]$  are the force states at  $\mathbf{x}$  and  $\mathbf{x}'$ , respectively, and when they act on the bonds  $\xi_{\mathbf{x}\mathbf{x}'}$  and  $\xi_{\mathbf{x}'\mathbf{x}}$  respectively, produces bond force density vectors acting at points  $\mathbf{x}$  and  $\mathbf{x}'$ , respectively. A material model  $\hat{\mathbf{T}}$  is then needed to ascribe to a bond a particular force density based on the deformation state at the point. Two class of material models arise in the state-based framework. When  $\hat{\mathbf{T}}$  is defined such that  $\mathbf{T}$  and  $\mathbf{Y}$  are colinear, then  $\hat{\mathbf{T}}$  is said to be ordinary state-based peridynamic material model, otherwise  $\hat{\mathbf{T}}$  is said to be non-ordinary state-based peridynamic material model. The non-ordinary state-based model provides a framework for modeling of more general material response. A subclass of the non-ordinary state-based model is called the *constitutive correspondence model*. This material model is becoming increasingly popular because it admits constitutive models from the classical continuum theory, thus making it possible to take advantage of the state-of-the-art in the well-established classical theory. Another advantage of the constitutive correspondence model that derives from its admittance of constitutive model from the classical theory is that it permits the use of familiar quantities such as stress and strain tensors within the peridynamic modeling framework.

The material model in the state-based framework is expressed such that the force vector state  $\mathbf{T}$  is related with appropriate physical quantities such as the deformation vector state  $\mathbf{Y}$ , the rate of deformation state  $\dot{\mathbf{Y}}$ , temperature  $T$ , damage  $\mathcal{D}$ , etc. The general form is given as:

$$\mathbf{T}[\mathbf{x}, t] = \hat{\mathbf{T}}[\mathbf{Y}, \dot{\mathbf{Y}}, T, \mathcal{D}, \dots] \quad (7)$$

The material model in the context of the non-ordinary constitutive framework is defined such that:

$$\mathbf{T} \langle \xi_{\mathbf{x}, \mathbf{x}'} \rangle = \omega \langle \xi \rangle \mathbf{P} \mathbf{K}^{-1} \xi_{\mathbf{x}, \mathbf{x}'} \quad (8)$$

where  $\omega$  is a scalar state which acts on the  $\xi$  to produce a scalar-valued influence function,  $\mathbf{P}$  is the first Piola stress tensor, and  $\mathbf{K}$  is a second order shape tensor defined as:

$$\mathbf{K} = \int_{\mathcal{H}_{\mathbf{x}}} \omega \langle \xi \rangle \xi \otimes \xi dV_{\xi} \quad (9)$$

## 2.2. Constitutive relation for the PD CONTACT model

The first Piola stress  $\mathbf{P}$  in (8) can be obtained from:

$$\mathbf{P} = J \boldsymbol{\sigma} \mathbf{F}^{-T}, \quad J = \det(\mathbf{F}) \quad (10)$$

where  $\boldsymbol{\sigma}$  is the Cauchy stress tensor and  $\mathbf{F}$  is the nonlocal deformation gradient defined as:

$$\mathbf{F}(\mathbf{x}) = \left[ \int_{\mathcal{H}_{\mathbf{x}}} \omega \langle \xi \rangle (\mathbf{y}(\mathbf{x}', t) - \mathbf{y}(\mathbf{x}, t)) \otimes \xi d\mathbf{x}' \right] \mathbf{K}^{-1} \quad (11)$$

It is worth noting that in the context of small deformation analysis, we have  $\mathbf{F} \cong \mathbf{I}$ ,  $J \cong 1$  and thus  $\mathbf{P} = \boldsymbol{\sigma}$  in (10). Since the constituents of the composite are viscoelastic and

owing to the capability of the non-ordinary state-based correspondence model to admit constitutive model from the classical theory, the hereditary integral constitutive model for linear isotropic non-ageing viscoelastic material will be utilized in this contribution, which expresses the time-dependent evolution of the Cauchy stress tensor  $\boldsymbol{\sigma}$  as:

$$\sigma_{ij}(t) = \int_0^t C_{ijkl}(t - \tau) \frac{d}{d\tau} \varepsilon_{kl}(\tau) d\tau \quad (12)$$

where  $C_{ijkl}(t - \tau)$  is the fourth order stress relaxation stiffness tensor and is usually estimated using a sequence of decaying exponents, which are also referred to as Prony series. The Prony series can be expressed as:

$$C_{ijkl}(t) = C_{ijkl\infty} + \sum_{m=1}^n C_{ijklm} \exp\left(-\frac{t}{\tau_m}\right) \quad (13)$$

## 2.3. Peridynamic computational homogenization theory

The PDCHT is a nonlocal first order homogenization that was proposed to facilitate the characterization of heterogeneous materials. The PDCHT is an effective homogenization framework composed of three main components: the definition of scale, localization, and development of homogenization rules.

### 2.3.1. Definition of scales

Definition of relevant scales of the problem is crucial in capturing the multiscale nature of materials with varying microstructures. It requires finding the appropriate level of description for the material at the microscale, where the microstructure is fully resolved, and at the macroscale, where the material is treated as homogeneous. Bearing in mind that the objective of PDCHT is to accurately characterize the effective response of a heterogeneous material  $M$ , composed of multiple constituent phases with varying properties. The task is then to find an equivalent substitute material  $\bar{M}$  that will exhibit the same bulk response as  $M$ . The basis for approximating material  $M$  with substitute material  $\bar{M}$  relies on two main assumptions. The first assumption is that if the individual phases in  $M$  display linear behavior, then the overall behavior of the substitute material  $\bar{M}$  will also be linear. Consequently, the constitutive function that connects stress and strain fields in  $\bar{M}$  follows a linear relationship of the form:

$$\bar{\sigma}_{ij}(t) = \bar{C}_{ijkl} \bar{\varepsilon}_{kl}(t) \quad (14)$$

where  $\bar{C}_{ijkl}$  represents the time dependent effective stiffness relaxation tensor. In (14) and throughout this communication, the overbar represents field variables related to the substitute homogeneous material  $\bar{M}$ , which is referred to as the macroscale.

The second assumption is the statistical homogeneity of the composite system  $M$ . This means that any randomly selected subregion of  $M$  that is large enough compared to individual microstructural elements or phases, such as the size of inclusions, exhibits the same average behavior as the

entire material [41]. These subregions are referred to as representative volume elements (RVEs) and represent the microscale for this homogenization scheme. Because the average properties of the composite material are the same within the RVE as they are in the entire material, the volume average of fields over the RVE can be used instead of the entire material.

### 2.3.2. Localization

This component consists of the dual steps of macro-micro transition in which the macroscopic stress or strain at a macroscopic point are transferred to the microscale to be used as boundary conditions of the microscale volume constraint problem, and solution of a volume constraint problem (VCP) at the microscale. The solution of the microscale VCP is achieved by implementing the Boltzmann viscoelastic model within the non-ordinary state-based correspondence peridynamic framework. The goal here is to utilize the macroscale fields as boundary conditions to simulate the behavior of the microstructure. As shown in [3], the admissible fields of stress, strain or displacement that can be applied as volume constraint to the microscale problem can be derived from the so-called nonlocal macrohomogeneity condition which is mathematically stated as:

$$\langle \sigma_{ij} \varepsilon_{ij} \rangle = \bar{\sigma}_{ij} \bar{\varepsilon}_{ij} \quad (15)$$

It was further demonstrated [3] that a sufficient condition for (15) to be satisfied, is to satisfy the so-called nonlocal Hill's lemma:

$$\langle \sigma_{ij} \varepsilon_{ij} \rangle - \bar{\sigma}_{ij} \bar{\varepsilon}_{ij} = \frac{1}{V_{\Omega_s}} \int_{\Omega_s} \int_{\Omega_c} ((\sigma_{ik} - \bar{\sigma}_{ik}) \mathcal{S}_{\omega}^s x_k (u_i - x_j \bar{\varepsilon}_{ij})) dV_{\Omega_s} \quad (16)$$

where  $\mathcal{S}_{\omega}^s$  represents a weighted nonlocal gradient operator,  $\omega(\mathbf{x}, \mathbf{x}') : \mathbb{R}^n \times \mathbb{R}^n \rightarrow \mathbb{R}^+$  is a weight function and the superscript  $S$  implies that  $\mathcal{S}$  is a symmetric gradient operator. For explanation on nonlocal gradient operator and general element of nonlocal vector calculus, refer to [3, 42]. The Hill's lemma (16), can be satisfied by using suitable boundary conditions. These conditions can include homogeneous displacement, homogeneous stress, and periodic boundary conditions. In this study, we will focus solely on the homogeneous displacement boundary condition, which is the most compatible with the peridynamic framework and easiest to implement. To achieve this condition, an appropriate displacement field is applied to the boundary of the representative volume element (RVE), causing the gradient of the displacement terms in the integrand of (16) to vanish. One way of vanishing the RHS of (16) is to apply linear displacement of the form:

$$\mathbf{u}(\mathbf{x}) = \bar{\boldsymbol{\varepsilon}} \mathbf{x} \quad \forall \mathbf{x} \in \Omega_c \quad (17)$$

### 2.3.3. Homogenization rules

The final component of the PDCHT is the development of homogenization rules that relate the macroscopic fields of stress and strain to the stress and strain fields at the

microscale. This component is essential for bridging the gap between the micro and macroscale and is the key to obtaining effective homogenization results. To this end, given the closed region  $\bar{\Omega} = \Omega_s \cup \Omega_c$  in which  $\Omega_s$  is the subregion where solution is sought and  $\Omega_c$  is the boundary region, the macroscopic and microscopic fields of stress and strains were shown [3] to be related through the so-called nonlocal average stress and strain theorems. Let the average stress and strain over  $\Omega_s$  be denoted respectively, as  $\langle \boldsymbol{\sigma} \rangle$  and  $\langle \boldsymbol{\varepsilon} \rangle$ , and let  $\bar{\boldsymbol{\sigma}}$  and  $\bar{\boldsymbol{\varepsilon}}$  be constant fields of stress and strain applied on  $\Omega_c$ , then the mathematical statement of the average stress and strain theorem are respectively given as:

$$\langle \boldsymbol{\sigma} \rangle = \bar{\boldsymbol{\sigma}} \quad (18)$$

and

$$\langle \boldsymbol{\varepsilon} \rangle = \bar{\boldsymbol{\varepsilon}} \quad (19)$$

where  $\langle \boldsymbol{\sigma} \rangle$  and  $\langle \boldsymbol{\varepsilon} \rangle$  are respectively given by:

$$\langle \boldsymbol{\sigma} \rangle = \frac{1}{V_{\Omega_s}} \int_{\Omega_s} \boldsymbol{\sigma}(\mathbf{x}_{\mu}) dV_{\Omega_s} \quad (20)$$

and

$$\langle \boldsymbol{\varepsilon} \rangle = \frac{1}{V_{\Omega_s}} \int_{\Omega_s} \boldsymbol{\varepsilon}(\mathbf{x}_{\mu}) dV_{\Omega_s} \quad (21)$$

Expressions (18) and (19) through (20) and (21) respectively allow the homogenized macroscopic stress and strain to be obtained as volume averages of the fields of microscopic stress and strains, respectively.

## 3. Numerical implementation

The application of the PDCHT to characterize the effective response of viscoelastic composites as proposed in [5] consists of the following steps:

1. Defining the RVE as the microscopic domain and finding its solutions. The solution of the microscopic IVCP will require solving (3) and the associated volume constraint (17) over the RVE. To achieve this numerically, the problem domain is discretized into a set of particles or nodes. Numerical methods such as finite element method (FEM) [43,44], meshfree methods [45,46], and collocation methods [47,48] are used to approximate the peridynamic model. The meshfree method proposed in [45] is particularly preferred in this contribution due to its simple implementation algorithm and relatively low computational cost. Using this approximation method, the discrete form of (3) is obtained as:

$$\rho_i \ddot{\mathbf{u}}_i = \sum_{j=1}^N \left[ \mathbf{T}[i, t] \langle \mathbf{x}_j - \mathbf{x}_i \rangle - \mathbf{T}[\mathbf{x}_j, t] \langle \mathbf{x}_i - \mathbf{x}_j \rangle \right] V_j + \mathbf{b}_i \quad (22)$$

where  $N$  is the number of nodes in the neighborhood of the primary node  $i$ .

2. Using volume averages of the micro fields of stress and strain to obtain the macroscopic stress and strain fields. This is achieved utilizing (20) and (21).



3. The effective stiffness relaxation tensor  $\overline{C}_{ijkl}$  is then extracted from the macroscopic stress and strains using (14).
4. Computing the effective viscoelastic material functions, such as the relaxation function from which the instantaneous and equilibrium relaxation are recovered.

#### 4. Numerical examples

A two-phase matrix-inclusion composite material consisting of a viscoelastic inclusion in a viscoelastic matrix is investigated. The viscoelastic material properties are given in Table 1. Two RVEs are studied. The first has a circular fiber and the second has an elliptical fiber as shown in Figure 1. The numerical studies are conducted over three cases of material phase contrast  $\varphi = 1/2$ ,  $\varphi = 1/4$  and  $\varphi = 1/6$ , where  $\varphi = k_{matrix}/k_{fibre}$ . For numerical implementation, the RVE is Discretized into a grid of 100 material points along each side.

Before proceeding with the main goal of this contribution, series of simulations will be undertaken to study the convergence of the numerical solutions under grid refinement. In undertaking this, the nonlocal length scale as represented by the horizon  $\delta$  is kept fixed. Convergence with respect to the internal length scale is not undertaken in this study as the choice of the horizon size has been shown to be in some relevant sense determined by the physics of the problem [49]. It was however demonstrated in [17] that a horizon size of 3 times the nodal spacing gives results that agree well with results from the classical local theory and would be adopted throughout this contribution.

The convergence study involved conducting simulations of an RVE with a circular inclusion over six different values of the nodal spacing,  $\Delta x = 0.1, 0.05, 0.033, 0.025, 0.02$ , and  $0.0167$ . The results obtained from these simulations are presented in Figure 2 and show that as the grid was progressively refined, the numerical solutions exhibited convergence behavior, with results from simulations corresponding to the grid sizes of  $0.025, 0.02$ , and  $0.0167$  showing high degree of agreement. This convergence trend indicates that further refinement of the grid beyond the grid size of  $0.025$  does not significantly impact the accuracy of the numerical solution.

Based on these findings, a grid size of  $0.02$  was determined to be appropriate for subsequent simulations. This choice ensures a balance between computational efficiency and accuracy in capturing the behavior of the viscoelastic composites under investigation. Additionally, a horizon size of  $\delta = 3.015\Delta x$  (where  $\Delta x$  is the nodal spacing) is adopted for the purpose of simulation throughout this

communication. This choice of horizon size has been demonstrated in previous studies [17] to yield results that align closely with simulations based on the local classical continuum theory.

With the appropriate grid size and horizon selected for the numerical simulations, the next step is to investigate the effect of phase contrast and inclusion shape on the effective properties of viscoelastic composites. In this respect, the components of the normalized effective instantaneous modulus for two cases of phase contrast are presented in Figure 3. The normalized effective instantaneous modulus is computed using:

$$\frac{E^*(t=0)}{E^m(t=0)} \quad (23)$$

where  $E^*(t=0)$  is the effective instantaneous relaxation modulus and  $E^m(t=0)$  is the instantaneous relaxation modulus of the matrix. From Figure 3, it was observed that the evolution of the components of the instantaneous modulus for the circular inclusion did not show anisotropy with an increase in volume fraction or with an increase in phase contrast. However, in the case of the elliptical inclusion, there was not only an appreciable degree of anisotropy with an increase in volume fraction, as expected, but there was also an increase in anisotropy with increasing phase contrast.

To quantify the degree of anisotropy, an anisotropy index,  $A$ , was computed for all cases using the expression [50],

$$A = \left( \left[ \frac{1}{4}(C_{11} + C_{22} + 2C_{12})(S_{11} + S_{22} + 2S_{12}) - 1 \right]^2 + 2 \left[ \frac{1}{6}(C_{11} + C_{22} - 2C_{12} + 4C_{66})(S_{11} + S_{22} - 2S_{12} + S_{66}) - 1 \right]^2 \right)^{\frac{1}{2}} \quad (24)$$

and the results are shown in Figure 4. The results in Figure 4 show the absence of anisotropy in the effective response of the viscoelastic composite with a circular inclusion, regardless of the magnitude of the phase contrast. However, for the RVE with an elliptical inclusion, an increase in the phase contrast corresponds to a higher anisotropy index. These results indicate that the elliptical inclusion has a more significant effect on the anisotropy of the composite material compared to a circular inclusion.

The effect of phase contrast on the equilibrium response of the viscoelastic composite system was investigated by computing the effective relaxation modulus of the RVEs with circular and elliptical fibers for the two cases of phase contrast corresponding to  $\varphi = 1/2$  and  $\varphi = 1/6$ . The results are presented in Figure 5, which shows that the effective equilibrium response of the RVE with circular fiber exhibits no anisotropy at equilibrium, whereas an appreciable anisotropy was observed in the case of the RVE with elliptical fiber.

To further analyze the anisotropy of the effective relaxation modulus tensor, Figure 6 presents the percentage difference between the components  $E_{11}^*$  and  $E_{22}^*$  of the

**Table 1.** Viscoelastic properties of the constituent materials.

| Iteration                | Phase  | $k_1$ | $k_2$ | $\tau_2$ | $\nu$ |
|--------------------------|--------|-------|-------|----------|-------|
| 1<br>( $\varphi = 1/2$ ) | Matrix | 1     | 10    | 10       | 0.38  |
|                          | Fiber  | 2     | 20    | 10       | 0.38  |
| 2<br>( $\varphi = 1/4$ ) | Matrix | 1     | 10    | 10       | 0.38  |
|                          | Fiber  | 4     | 40    | 10       | 0.38  |
| 3<br>( $\varphi = 1/6$ ) | Matrix | 1     | 10    | 10       | 0.38  |
|                          | Fiber  | 6     | 60    | 10       | 0.38  |

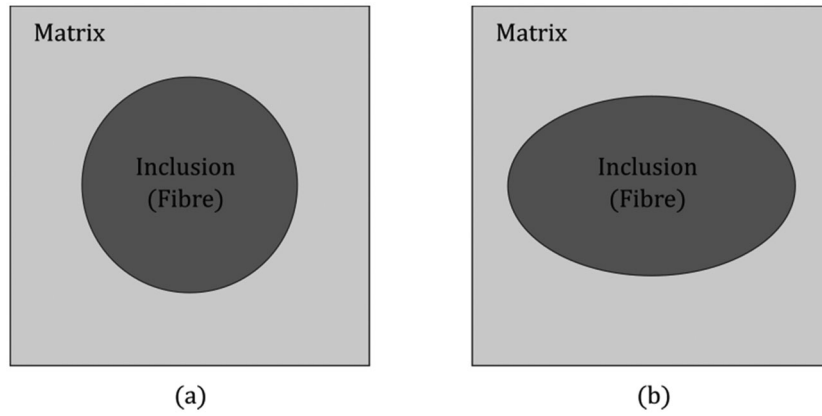


Figure 1. RVE of the composite systems: (a) circular inclusion, and (b) elliptical inclusion.

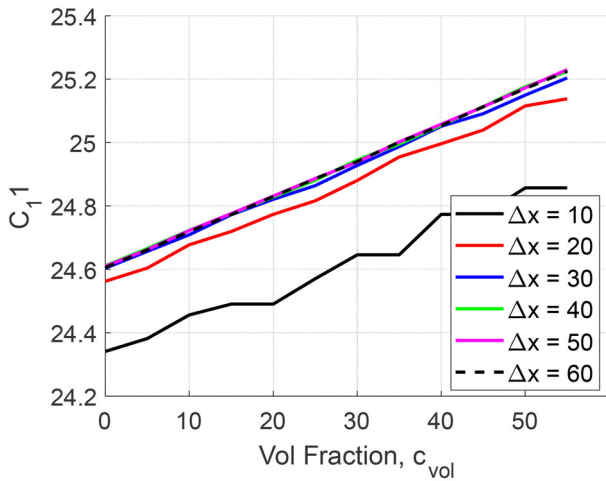


Figure 2. Convergence study: effect of grid size on  $C_{11}$  component of the effective instantaneous modulus of the RVE with circular inclusion.

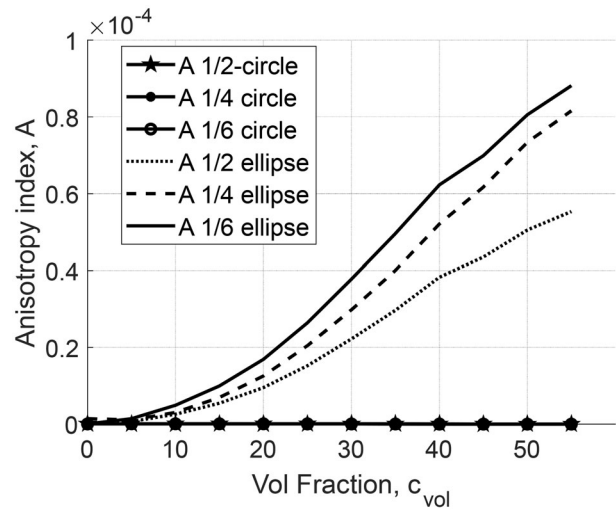


Figure 4. Elastic anisotropy index for both RVEs.

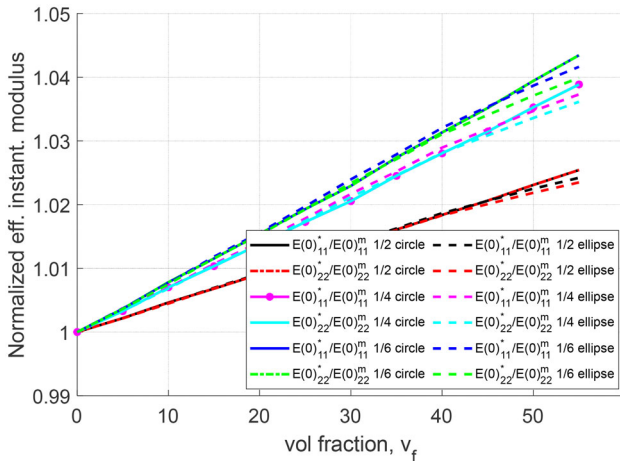


Figure 3. Components of normalized effective instantaneous modulus for the two cases of phase contrast.

relaxation modulus tensor. It is observed that the effective relaxation modulus tensor of the RVE with circular inclusion exhibits isotropic behavior for all cases of the phase contrast. However, the effective relaxation modulus tensor of the RVE with elliptical fiber exhibits an anisotropic response, and the degree of anisotropy increases with an increase in phase contrast.

### 5. Summary and conclusion

This paper investigates the influence of inclusion shape and phase contrast on the effective response of viscoelastic composites using Peridynamic Computational Homogenization Theory. The study is motivated by the fact that inclusion shape can vary widely during the production of composite materials, and understanding the nature and degree of the influence of inclusion shape on the effective response of the composite system is essential in meeting specific property requirements. Furthermore, the difference in physical properties between the matrix and the inclusion, known as phase contrast, also affects the effective response of the composite system. The paper extends the application of nonlocal first-order Peridynamic computational homogenization theory proposed in previous studies to investigate the dual influence of phase stiffness contrast and inclusion shape on the effective response of viscoelastic composites.

This study has demonstrated that the inclusion shape and phase contrast have a significant influence on the effective response of viscoelastic composites. The numerical investigation was carried out on a two-phase matrix-inclusion composite material with viscoelastic properties. To study the influence of the phase contrast and inclusion shape on the instantaneous effective properties of the composite systems,

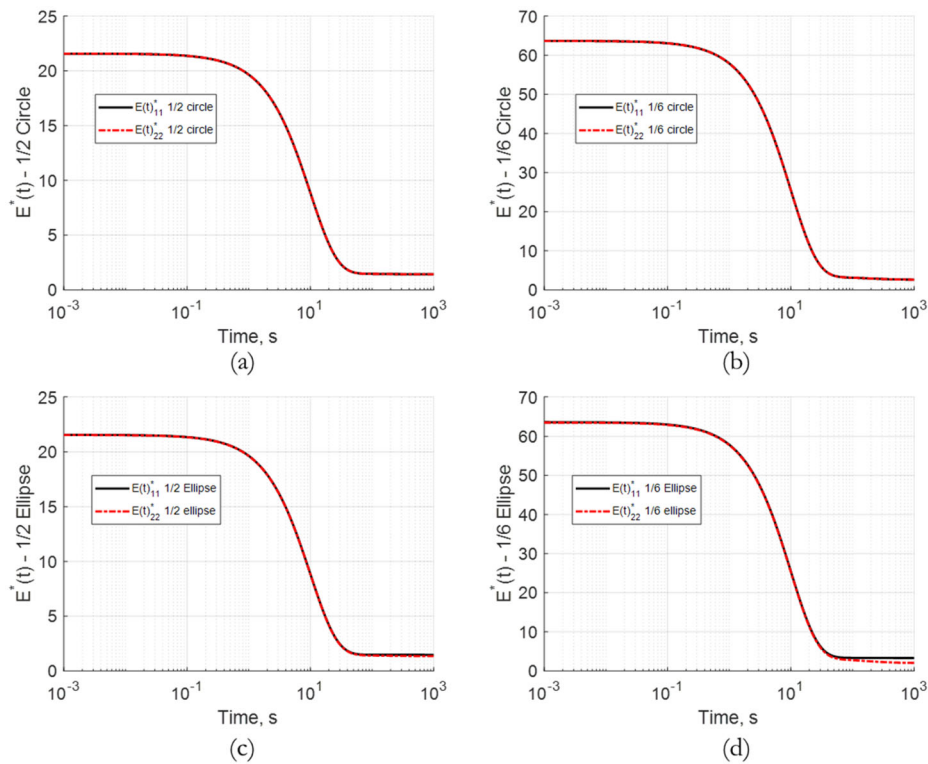


Figure 5. Effect of phase contrast on the effective equilibrium response of the viscoelastic composite systems.

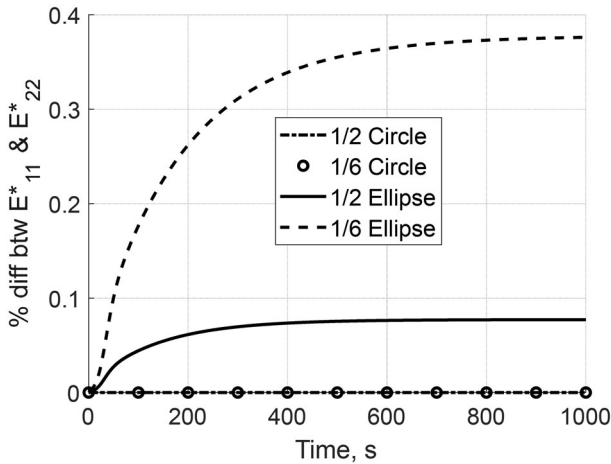


Figure 6. Difference in the components of the effective relaxation modulus tensor.

this study considered three cases of material phase contrast,  $\varphi = 1/2$ ,  $\varphi = 1/4$  and  $\varphi = 1/6$ . The simulation results showed that the effective instantaneous relaxation modulus in RVE with circular inclusion remained isotropic for all phase contrasts. However, for the RVE with elliptical inclusion, the effective relaxation modulus showed anisotropy, which increased with the increase in phase contrast. Furthermore, the effective relaxation modulus for the RVE with circular inclusion showed isotropic relaxation at equilibrium, for two cases of phase contrasts  $\varphi = 1/2$  and  $\varphi = 1/6$  while the RVE with elliptical inclusion showed anisotropic relaxation at equilibrium, which increased as the phase contrast increases from  $\varphi = 1/2$  to  $\varphi = 1/6$ . The increase in anisotropy is deemed large enough to be considered when estimating the characteristics of a new composite.

These findings have shed light on the effective behavior of viscoelastic composites under different phase contrasts, as well as the influence of inclusion geometry. However, there are still several areas that could be explored in future research. Some key areas to explore include investigating different inclusion shapes beyond circular and elliptical, such as rectangular, triangular, or irregular shapes. This would provide a more comprehensive understanding of how different geometries influence the effective response of the composites.

To further strengthen the findings presented in this paper, experimental validation of the numerical results is recommended. Conducting mechanical testing, imaging, and microscopy studies to measure and analyze the effective response of viscoelastic composites over a range of phase contrasts and inclusion shapes would enhance the credibility of the findings and provide a basis for practical applications.

Finally, exploring the impact of other material properties, such as interfacial properties, viscoelastic relaxation times, or non-linear behavior, on the effective behavior of viscoelastic composites is another area of future research. This would enhance our understanding of composites and enable more precise predictions of their effective response.

## Acknowledgments

The first author is supported by the government of the federal republic of Nigeria through the Petroleum Technology Development Fund (PTDF). The authors acknowledge the British Council for supporting the UK-Egypt Higher Education Climate Change Partnerships project No. 12 (Towards A Sustainable Strategy Framework to Confront Climate Change for The Water Sector Powered by Renewable Energy in Egypt).

## Disclosure statement

The authors have no competing interests to declare that are relevant to the content of this article.

## ORCID

Selda Oterkus  <http://orcid.org/0000-0002-4614-7214>

## References

- [1] I.V. Magnitsky, and E.S. Sergeeva, *Influence of the inclusion shape on the effective elastic properties of composites*, IOP Conference Series: Materials Science and Engineering, 2019. **489**(1): p. 012007. DOI: [10.1088/1757-899X/489/1/012007](https://doi.org/10.1088/1757-899X/489/1/012007).
- [2] Y. Luo, *Improved Voigt and Reuss Formulas with the Poisson Effect*, Materials., vol. 15, no. 16, pp. 5656, 2022. DOI: [10.3390/ma15165656](https://doi.org/10.3390/ma15165656).
- [3] Y.K. Galadima, W. Xia, E. Oterkus, and S. Oterkus, *A computational homogenization framework for non-ordinary state-based peridynamics*, Eng. Comput., vol. 39, no. 1, pp. 461–487, 2023. DOI: [10.1007/s00366-021-01582-6](https://doi.org/10.1007/s00366-021-01582-6).
- [4] Y.K. Galadima, W. Xia, E. Oterkus, and S. Oterkus, *Peridynamic computational homogenization theory for materials with evolving microstructure and damage*, Eng. Comput., 2022. DOI: [10.1007/s00366-022-01696-5](https://doi.org/10.1007/s00366-022-01696-5).
- [5] Y.K. Galadima, S. Oterkus, E. Oterkus, I. Amin, A.-H. El-Aassar, and H. Shawky, *A Nonlocal Method to Compute Effective Properties of Viscoelastic Composite Materials Based on Peridynamic Computational Homogenization Theory*, Compos. Struct., vol. 319, pp. 117147, 2023. DOI: [10.1016/j.compstruct.2023.117147](https://doi.org/10.1016/j.compstruct.2023.117147).
- [6] A. Pagani, R. Augello, and E. Carrera, *Numerical simulation of deployable ultra-thin composite shell structures for space applications and comparison with experiments*, Mech. Adv. Mater. Struct., vol. 30, no. 8, pp. 1591–1603, 2023. DOI: [10.1080/15376494.2022.2037173](https://doi.org/10.1080/15376494.2022.2037173).
- [7] M. Cinefra, A.G. de Miguel, M. Filippi, C. Houriet, A. Pagani, and E. Carrera, *Homogenization and free-vibration analysis of elastic metamaterial plates by Carrera Unified Formulation finite elements*, Mech. Adv. Mater. Struct., vol. 28, no. 5, pp. 476–485, 2021. DOI: [10.1080/15376494.2019.1578005](https://doi.org/10.1080/15376494.2019.1578005).
- [8] T.-D. Nguyen, S.-T. Nguyen, and T.-H. Tran, *An asymptotic generalized self-consistent scheme for the effective rheological properties of viscoelastic composites*, Mech. Adv. Mater. Struct., vol. 26, no. 23, pp. 1969–1980, 2019. DOI: [10.1080/15376494.2018.1455936](https://doi.org/10.1080/15376494.2018.1455936).
- [9] T. Nguyen-Sy, and T.-D. Nguyen, *On the effective properties of composites made of viscoelastic constituents*, Mech. Adv. Mater. Struct., vol. 28, no. 13, pp. 1328–1336, 2021. DOI: [10.1080/15376494.2019.1668093](https://doi.org/10.1080/15376494.2019.1668093).
- [10] J. Qu, K. Khan, S. Meng, and A. Muliana, *Modeling nonlinear viscoelastic responses of flexible composites for soft robotics applications*, Mech. Adv. Mater. Struct., pp. 1–13, 2022. DOI: [10.1080/15376494.2022.2063460](https://doi.org/10.1080/15376494.2022.2063460).
- [11] S.A. Silling, *Reformulation of elasticity theory for discontinuities and long-range forces*, J. Mech. Phys. Solids., vol. 48, no. 1, pp. 175–209, 2000. DOI: [10.1016/S0022-5096\(99\)00029-0](https://doi.org/10.1016/S0022-5096(99)00029-0).
- [12] M. Imachi, S. Tanaka, T.Q. Bui, S. Oterkus, and E. Oterkus, *A computational approach based on ordinary state-based peridynamics with new transition bond for dynamic fracture analysis*, Eng. Fract. Mech., vol. 206, pp. 359–374, 2019. DOI: [10.1016/j.engfracmech.2018.11.054](https://doi.org/10.1016/j.engfracmech.2018.11.054).
- [13] M. Imachi, S. Tanaka, M. Ozdemir, T.Q. Bui, S. Oterkus, and E. Oterkus, *Dynamic crack arrest analysis by ordinary state-based peridynamics*, Int. J. Fract., vol. 221, no. 2, pp. 155–169, 2020. DOI: [10.1007/s10704-019-00416-3](https://doi.org/10.1007/s10704-019-00416-3).
- [14] O. Karpenko, S. Oterkus, and E. Oterkus, *Peridynamic investigation of the effect of porosity on fatigue nucleation for additively manufactured titanium alloy Ti6Al4V*, Theor. Appl. Fract. Mech., vol. 112, pp. 102925, 2021. DOI: [10.1016/j.tafmec.2021.102925](https://doi.org/10.1016/j.tafmec.2021.102925).
- [15] A. Kefal, A. Sohoul, E. Oterkus, M. Yildiz, and A. Suleman, *Topology optimization of cracked structures using peridynamics*, Continuum Mech. Thermodyn., vol. 31, no. 6, pp. 1645–1672, 2019. DOI: [10.1007/s00161-019-00830-x](https://doi.org/10.1007/s00161-019-00830-x).
- [16] X. Liu, X. He, J. Wang, L. Sun, and E. Oterkus, *An ordinary state-based peridynamic model for the fracture of zigzag graphene sheets*, Proceedings of the Royal Society A: Mathematical, Physical and Engineering Sciences, 2018. **474**(2217): p. 20180019.
- [17] E. Madenci, and E. Oterkus, *Peridynamic Theory and Its Applications*, 2014. New York, United States Springer, New York.
- [18] C.T. Nguyen, S. Oterkus, and E. Oterkus, *An energy-based peridynamic model for fatigue cracking*, Eng. Fract. Mech., vol. 241, pp. 107373, 2021. DOI: [10.1016/j.engfracmech.2020.107373](https://doi.org/10.1016/j.engfracmech.2020.107373).
- [19] E. Oterkus, and E. Madenci, *Peridynamic Theory for Damage Initiation and Growth in Composite Laminate*, KEM., vol. 488–489, pp. 355–358, 2011. DOI: [10.4028/www.scientific.net/KEM.488-489.355](https://doi.org/10.4028/www.scientific.net/KEM.488-489.355).
- [20] E. Oterkus, E. Madenci, O. Weckner, S. Silling, P. Bogert, and A. Tessler, *Combined finite element and peridynamic analyses for predicting failure in a stiffened composite curved panel with a central slot*, Compos. Struct., vol. 94, no. 3, pp. 839–850, 2012. DOI: [10.1016/j.compstruct.2011.07.019](https://doi.org/10.1016/j.compstruct.2011.07.019).
- [21] Bozo Vazic, Hanlin Wang, Cagan Diyaroglu, Selda Oterkus, and Erkan Oterkus, S. Oterkus, and E. Oterkus, *Dynamic propagation of a macrocrack interacting with parallel small cracks*, AIMS Material Science., vol. 4, no. 1, pp. 118–136, 2017. DOI: [10.3934/mat.2017.1.118](https://doi.org/10.3934/mat.2017.1.118).
- [22] H. Wang, E. Oterkus, and S. Oterkus, *Three-Dimensional Peridynamic Model for Predicting Fracture Evolution during the Lithiation Process*, 2018.
- [23] X. Zhang, Z. Xu, and Q. Yang, *Wave Dispersion and Propagation in Linear Peridynamic Media*, Shock Vib., vol. 2019, pp. 9528978, 2019.
- [24] X. Gu, Q. Zhang, D. Huang, and Y. Yv, *Wave dispersion analysis and simulation method for concrete SHPB test in peridynamics*, Eng. Fract. Mech., vol. 160, pp. 124–137, 2016. DOI: [10.1016/j.engfracmech.2016.04.005](https://doi.org/10.1016/j.engfracmech.2016.04.005).
- [25] A. Keramat, and A. Ahmadi, *Axial wave propagation in viscoelastic bars using a new finite-element-based method*, J. Eng. Math., vol. 77, no. 1, pp. 105–117, 2012. DOI: [10.1007/s10665-012-9556-y](https://doi.org/10.1007/s10665-012-9556-y).
- [26] S. Kulkarni, and A. Tabarraei, *An analytical study of wave propagation in a peridynamic bar with nonuniform discretization*, Eng. Fract. Mech., vol. 190, pp. 347–366, 2018. DOI: [10.1016/j.engfracmech.2017.12.019](https://doi.org/10.1016/j.engfracmech.2017.12.019).
- [27] S.A. Silling, *Attenuation of waves in a viscoelastic peridynamic medium*, Math. Mech. Solids., vol. 24, no. 11, pp. 3597–3613, 2019. DOI: [10.1177/1081286519847241](https://doi.org/10.1177/1081286519847241).
- [28] R.A. Wildman, and G.A. Gazonas, *A finite difference-augmented peridynamics method for reducing wave dispersion*, Int. J. Fract., vol. 190, no. 1–2, pp. 39–52, 2014. DOI: [10.1007/s10704-014-9973-1](https://doi.org/10.1007/s10704-014-9973-1).
- [29] Y. Galadima, E. Oterkus, and S. Oterkus, *Department of Naval Architecture, Ocean and Marine Engineering, University of Strathclyde, 100 Montrose Street, Glasgow G4 0LZ, UK, Two-dimensional implementation of the coarsening method for linear peridynamics*, AIMS Mater. Sci., vol. 6, no. 2, pp. 252–275, 2019. DOI: [10.3934/mat.2019.2.252](https://doi.org/10.3934/mat.2019.2.252).
- [30] Y.K. Galadima, E. Oterkus, and S. Oterkus, *Model order reduction of linear peridynamic systems using static condensation*, Math. Mech. Solids., vol. 26, no. 4, pp. 552–569, 2021. DOI: [10.1177/1081286520937045](https://doi.org/10.1177/1081286520937045).



- [31] Y.K. Galadima, E. Oterkus, and S. Oterkus, *Static condensation of peridynamic heat conduction model*, *Math. Mech. Solids.*, vol. 27, no. 12, pp. 2689–2714, 2022. DOI: [10.1177/10812865221081160](https://doi.org/10.1177/10812865221081160).
- [32] Y.K. Galadima, W. Xia, E. Oterkus, and S. Oterkus, *Chapter 17 - Multiscale modeling with peridynamics*. in *Peridynamic Modeling, Numerical Techniques, and Applications*, E. Oterkus, S. Oterkus, and E. Madenci, Editors., 2021. Elsevier, Amsterdam, Netherlands. p. 371–386
- [33] Y.K. Galadima, E. Oterkus, and S. Oterkus, *Investigation of the effect of shape of inclusions on homogenized properties by using peridynamics*, *Proced. Struct. Integrity.*, vol. 28, pp. 1094–1105, 2020. DOI: [10.1016/j.prostr.2020.11.124](https://doi.org/10.1016/j.prostr.2020.11.124).
- [34] W. Xia, Y. Galadima, E. Oterkus, and S. Oterkus, *Representative volume element homogenization of a composite material by using bond-based peridynamics*, *J. Compos. Biodegrad. Polym.*, vol. 7, pp. 51–56, 2019. DOI: [10.12974/2311-8717.2019.07.7](https://doi.org/10.12974/2311-8717.2019.07.7).
- [35] Y.K. Galadima, S. Oterkus, E. Oterkus, I. Amin, A.-H. El-Aassar, and H. Shawky, *Modelling of viscoelastic materials using non-ordinary state-based peridynamics*, *Eng. Comput.*, 2023. DOI: [10.1007/s00366-023-01808-9](https://doi.org/10.1007/s00366-023-01808-9).
- [36] O. Weckner, and N.A. Nik Mohamed, *Viscoelastic material models in peridynamics*, *Appl. Math. Comput.*, vol. 219, no. 11, pp. 6039–6043, 2013. DOI: [10.1016/j.amc.2012.11.090](https://doi.org/10.1016/j.amc.2012.11.090).
- [37] D. Behera, P. Roy, and E. Madenci, *Peridynamic modeling of bonded-lap joints with viscoelastic adhesives in the presence of finite deformation*, *Comput. Methods Appl. Mech. Eng.*, vol. 374, pp. 113584, 2021. DOI: [10.1016/j.cma.2020.113584](https://doi.org/10.1016/j.cma.2020.113584).
- [38] E. Madenci, and S. Oterkus, *Ordinary state-based peridynamics for plastic deformation according to von Mises yield criteria with isotropic hardening*, *J. Mech. Phys. Solids.*, vol. 86, pp. 192–219, 2016. DOI: [10.1016/j.jmps.2015.09.016](https://doi.org/10.1016/j.jmps.2015.09.016).
- [39] X. Zhou, and T. Zhang, *Generalized plastic ordinary state-based peridynamic model with shear deformation of geomaterials*, *Acta Geotech.*, vol. 18, no. 2, pp. 609–623, 2023. DOI: [10.1007/s11440-022-01626-1](https://doi.org/10.1007/s11440-022-01626-1).
- [40] S.A. Silling, M. Epton, O. Weckner, J. Xu, and E. Askari, *Peridynamic States and Constitutive Modeling*, *J. Elasticity.*, vol. 88, no. 2, pp. 151–184, 2007. DOI: [10.1007/s10659-007-9125-1](https://doi.org/10.1007/s10659-007-9125-1).
- [41] Z. Hashin, *Viscoelastic Behavior of Heterogeneous Media*, *J. Appl. Mech.*, vol. 32, no. 3, pp. 630–636, 1965. DOI: [10.1115/1.3627270](https://doi.org/10.1115/1.3627270).
- [42] Q. Du, M. Gunzburger, R.B. Lehoucq, and K. Zhou, *A Nonlocal Vector Calculus, Nonlocal Volume-Constrained Problems, and Nonlocal Balance Laws*, *Math. Models Methods Appl. Sci.*, vol. 23, no. 03, pp. 493–540, 2013. DOI: [10.1142/S0218202512500546](https://doi.org/10.1142/S0218202512500546).
- [43] X. Chen, and M. Gunzburger, *Continuous and discontinuous finite element methods for a peridynamics model of mechanics*, *Comput. Methods Appl. Mech. Eng.*, vol. 200, no. 9–12, pp. 1237–1250, 2011. DOI: [10.1016/j.cma.2010.10.014](https://doi.org/10.1016/j.cma.2010.10.014).
- [44] H. Wang, and H. Tian, *A fast Galerkin method with efficient matrix assembly and storage for a peridynamic model*, *Comput. Phys.*, vol. 231, no. 23, pp. 7730–7738, 2012. DOI: [10.1016/j.jcp.2012.06.009](https://doi.org/10.1016/j.jcp.2012.06.009).
- [45] S.A. Silling, and E. Askari, *A meshfree method based on the peridynamic model of solid mechanics*, *Comput. Struct.*, vol. 83, no. 17–18, pp. 1526–1535, 2005. DOI: [10.1016/j.compstruc.2004.11.026](https://doi.org/10.1016/j.compstruc.2004.11.026).
- [46] M.L. Parks, R.B. Lehoucq, S.J. Plimpton, and S.A. Silling, *Implementing peridynamics within a molecular dynamics code*, *Comput. Phys. Commun.*, vol. 179, no. 11, pp. 777–783, 2008. DOI: [10.1016/j.cpc.2008.06.011](https://doi.org/10.1016/j.cpc.2008.06.011).
- [47] H. Wang, and H. Tian, *A fast and faithful collocation method with efficient matrix assembly for a two-dimensional nonlocal diffusion model*, *Comput. Methods Appl. Mech. Eng.*, vol. 273, pp. 19–36, 2014. DOI: [10.1016/j.cma.2014.01.026](https://doi.org/10.1016/j.cma.2014.01.026).
- [48] G.I. Evangelatos, and P.D. Spanos, *A collocation approach for spatial discretization of stochastic peridynamic modeling of fracture*, *J. Mech. Mater. Struct.*, vol. 6, no. 7–8, pp. 1171–1195, 2011. DOI: [10.2140/jomms.2011.6.1171](https://doi.org/10.2140/jomms.2011.6.1171).
- [49] F. Bobaru, M. Yang, L.F. Alves, S.A. Silling, E. Askari, and J. Xu, *Convergence, adaptive refinement, and scaling in 1D peridynamics*, *Int. J. Numer. Meth. Engng.*, vol. 77, no. 6, pp. 852–877, 2009. DOI: [10.1002/nme.2439](https://doi.org/10.1002/nme.2439).
- [50] R. Li, Q. Shao, E. Gao, and Z. Liu, *Elastic anisotropy measure for two-dimensional crystals*, *Extreme Mech. Lett.*, vol. 34, pp. 100615, 2020. DOI: [10.1016/j.eml.2019.100615](https://doi.org/10.1016/j.eml.2019.100615).